Available online at www.sciencedirect.com
SCIENCE DIRECT
Journal of Power Sources 155 (2006) 128–137
JOURNAL OF POWER SOURCES
www.elsevier.com/locate/jpowsour

Chemical interaction between glass–ceramic sealants and interconnect steels in SOFC stacks

P. Batfalsky [a], V.A.C. Haanappel [b,*], J. Malzbender [b], N.H. Menzler [b], V. Shemet [b], I.C. Vinke [b], R.W. Steinbrech [b]

[a] *Central Department of Technology, Forschungszentrum Jülich, D-52425 Jülich, Germany*
[b] *Institute for Materials and Processes in Energy Systems, Forschungszentrum Jülich, D-52425 Jülich, Germany*

Received 22 November 2004; accepted 2 May 2005
Available online 18 July 2005

Abstract

In order to gain insight into the mechanism causing performance degradation and/or failure, stacks of planar solid oxide fuel cells (SOFC) are routinely dismantled and examined after operation at Forschungszentrum Jülich. The post-operation inspection focuses in particular on the chemical and mechanical compatibility aspects of cell and stack materials.

In the present work a short-term degradation effect is addressed, which was found to be caused by unwanted chemical interactions between glass–ceramic sealants and ferritic steel interconnects. The post-operation inspection revealed severe steel corrosion along the seal rims. Under SOFC stack conditions rapidly growing oxide nodules were observed bridging the 200 μm seal gap between the metallic components after a few hundred hours of operation. These oxide nodules, rich in iron, gave rise to local short-circuiting effects eventually resulting in stack failure.

The present study, combined with recent model investigations triggered by the stack results, indicates that severe degradation only occurs in the case of glass–ceramic sealants which contain minor amounts of PbO. Furthermore, the rate of corrosion attack of the metallic components strongly depends on the silicon (Si) content of the ferritic steel. The stack tests suggest that increasing the Si content increases the corrosion rate, and thus detrimentally influences the stack performance.
© 2005 Elsevier B.V. All rights reserved.

Keywords: SOFC stacks; Glass–ceramic sealants; Interconnect materials; Ferritic high-chromium steels; Chemical interaction; Short-circuiting

1. Introduction

Research and development activities at Forschungszentrum Jülich (FZJ) on solid oxide fuel cells (SOFCs) concentrate on a planar design concept that offers high surface, volumetric and gravimetric power densities [1]. Standard cells to be used for SOFC stacks comprise thick anode substrates of Ni–yttria–stabilized zirconia (YSZ) cermets, thin YSZ electrolytes and lanthanum–strontium–iron–cobalt or lanthanum–strontium–manganite cathodes [2]. These cells are embedded in metallic frames of a high-chromium-containing ferritic steel and are stacked in serial mode using bipolar metallic interconnects [1].

The rigid fixation of the cells in the metallic frame and the sealing of the anode and cathode compartments are provided by glass–ceramics. Variants of the BCAS ($BaO–CaO–Al_2O_3–SiO_2$) system are used for joining the dissimilar and similar materials, i.e. ceramic cells, metallic manifolds, and metallic interconnects [3–6]. Besides electrical insulation and gas-tightness, these sealants are also tailored for satisfactory matching of the thermal expansion with the cell and steel components [4,7].

To date several high-temperature corrosion-resistant metallic alloys have been investigated as interconnect materials [8–16]. Low-cost interconnecting of the stack planes is

* Corresponding author. Tel.: +49 2461 614656; fax: +49 2461 616770.
E-mail address: v.haanappel@fz-juelich.de (V.A.C. Haanappel).

0378-7753/$ – see front matter © 2005 Elsevier B.V. All rights reserved.
doi:10.1016/j.jpowsour.2005.05.046

realized at FZJ by a specially developed ferritic steel with ~22 wt.% chromium content [15,16]. This steel, which is meanwhile also available as a commercial product (Crofer22APU, Thyssen–Krupp, Germany), matches in thermal expansion that of the anode substrate, has sufficient electrical conductivity, and forms a thin double-layered oxide scale at SOFC operation temperatures [13].

However, considering the variation of glass–ceramic and steel compositions tested in the past in FZJ stacks, there have also been some combinations which exhibited pronounced chemical interaction causing severe stack degradation. In particular, stacks that failed due to short-circuiting after only a few hundred hours of operation at 800 °C were of the greatest interest for post-operation analyses [17–19].

The present work aims to elucidate this unfavourable short-term malfunctioning of SOFC stacks. The electrochemical performance of the stacks is illustrated and results of post-operation stack examinations are presented. The assumed chemical interaction mechanism is compared with the findings of follow-up high-temperature model experiments [20–22]. These tests, recently carried out with sealed steel plates under various atmospheres, demonstrated unambiguously the importance of small differences in the chemical composition of glass–ceramic sealants and ferritic steels. In addition, the influence of operation temperature on the reaction kinetics was demonstrated. Finally, material-based strategies are discussed to eliminate or at least to suppress short-term degradation of SOFC stacks.

2. Experimental

2.1. Stack design

In the present work only SOFC stacks in F-design [23] are considered. Fig. 1 shows a schematic view of a two-cell stack variant with internal manifolds and counterflow. The fuel and oxidant enter the stack from the bottom through two tubes each. Channels in the interconnect distribute the air over the surface of the cathode. The electrical contact between the cathode and the interconnect was provided by a thin contact layer of a perovskite-type oxide. At the anode side, a coarse nickel mesh provides the electrical contact between the anode substrate of the cell and the interconnect. This nickel mesh also gives the fuel access to the anode substrate surface. In the exit manifolds the gases are collected and leave the stack through one central tube on each side. In the F-design the cells are fixed in a metal frame with a glass–ceramic sealant. The metallic interconnects and frames are joined together with the same glass–ceramic material. Fig. 1 illustrates the tracks of the glass–ceramic sealant on the stack planes.

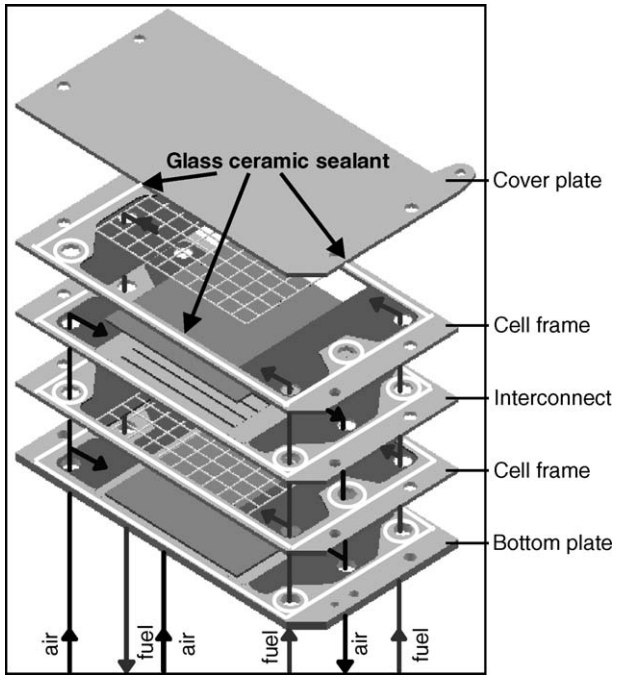

Fig. 1. Schematic view of a two-plane SOFC stack of F-design (FZJ).

2.2. Materials

The stacks were assembled from two high-chromium ferritic steels, referred to as Crofer22APU-1st and JS-3. Note that the addition -1st was chosen to distinguish the steel from the current commercial Crofer22APU variant. JS reflects the original Jülich steel development. The chemical compositions of the ferritic steels (Table 1) were similar except that the Si and Al contents were one order of magnitude higher for Crofer22APU-1st (0.1 wt.%) compared to JS-3 (<0.01 wt.%).

Glass–ceramic sealants based on the BCAS system (BaO, CaO, Al_2O_3, SiO_2) were used. They also contained minor additions of transition metal oxides, such as ZnO, PbO, and/or V_2O_5 to adjust the SOFC relevant physical and chemical properties. Table 2 shows the chemical composition of the

Table 2
Chemical composition of the various glass sealants used

Glass sealant	SiO_2	CaO	BaO	Small amounts of additives
A	34.7	8.6	41.4	Al_2O_3, ZnO, PbO, B_2O_3, V_2O_5
D	27.9	5.7	49.1	Al_2O_3, ZnO, PbO, B_2O_3, V_2O_5

Table 1
Chemical composition of the alloys used

Alloy	Fe	Cr	Mn	Ti	Si	Al	Re-el.	Ni
Crofer22APU-1st	Bal.	22.6	0.4	0.06	0.1	0.1	La-0.1	0.2
JS-3	Bal.	23.3	0.4	0.05	<0.01	<0.01	La-0.1	–

Table 3
Overview of the various stacks tested including steel and glass–ceramic type

Stack type	Steel type	Glass–ceramic
A	Crofer22APU-1st	A
B	JS-3	D
C	JS-3	A
D	Crofer22APU-1st (+8YSZ)	A

two glass–ceramic batches used, "A" and "D". All sealants were dispenser-deposited at room temperature on the SOFC components as a glass paste.

Besides the compositional variations of glass–ceramic sealants and ferritic steels, one stack was also assembled with cell frames coated by plasma-sprayed 7–8 wt.% yttria stabilized zirconia (YSZ). The use of a coating was intended to suppress unwanted physical and chemical interactions between the glass–ceramic and the ferritic steel.

The manifold at the cathode side was coated with a protective oxide layer (composition similar to the contact layer).

The glass–ceramic–ferritic steel combinations of otherwise geometrically identical stacks are listed in Table 3.

2.3. Cells

The SOFCs had either $La_{0.65}Sr_{0.3}MnO_3$ (LSM)/8YSZ cathodes with an LSM cathode current collector layer, or lanthanum–strontium–iron–cobalt-based (LSFC) cathodes with a ceria–gadolinia (CGO) diffusion barrier. At 700 °C SOFCs with LSFC cathodes exhibit an electrochemical performance comparable to LSM cathodes at 800 °C. More information about this type of cathode can be found elsewhere [2,24].

2.4. Joining of stacks

The interconnect components were joined and the SOFCs fixed in the metallic frame by using a specified thermal treatment of the sealant and simultaneously applying a mechanical load. During the entire joining procedure, the anode compartment was flushed with argon in order to prevent oxidation of the Ni mesh.

2.5. Electrochemical measurements

After reduction of the anode by stepwise replacement of the argon flow by hydrogen saturated with 10 vol.% water vapour, the open cell voltage (OCV) was measured. After the OCV check and I–V measurements the SOFC stack was operated at the desired temperature under a constant electrical load of 0.3 A cm^{-2}. The degradation behaviour of the stack was monitored by means of the output cell voltage as a function of the operation time. Fuel utilization during steady-state operation was always less than 10%. The stack tests were terminated after either strong progressive degradation or short-circuiting between individual stack planes.

2.6. Post-operation inspection and characterization

All stacks were examined after operation. As preparation techniques either plane-by-plane dismantling or infiltration with a resin and metallographic polishing of cross sections was used to gain access to the locations of chemical interaction. Optical microscope images were taken at the relevant interaction sites. In addition, scanning electron microscopy (SEM) provided detailed images of the surface morphology and cross sections. SEM work was performed using a LEICA S360 electron microscope equipped with an EDX (Oxford Instruments) analysis system.

3. Results

3.1. Electrochemical performance

Fig. 2 shows the time dependence of the cell voltage of a type A stack (ferritic steel Crofer22APU-1st with glass–ceramic "A") during operation at 800 °C. The current density was set at 0.3 A cm^{-2}. Starting from a cell voltage of about 860 mV, a rapid decrease to a value below 800 mV is observed, characteristic of the initial adjustments of the materials in the conductive chain. After about 170 h of operation, the stack exhibited a sharp decrease in cell voltage to less than 200 mV.

The electrochemical performance of other stacks with the same material combination, Crofer22APU-1st/"A", confirmed that short-term degradation effects already occur after a few hundred hours of operation at 800 °C. The OCV measured thereafter was often much lower than the theoretical value according to the Nernst equation. In these cases, the ohmic resistance at room temperature across certain stack planes was as low as 1–3 Ω, indicative of short-circuiting. Non-published results have shown that a decrease of the stack operation temperature to 700 °C delayed the onset of rapid degradation by a factor 10–20.

Similar to the extended life at lower temperature, type B (JS-3 with "D") and type C (JS-3 with "A") stacks displayed

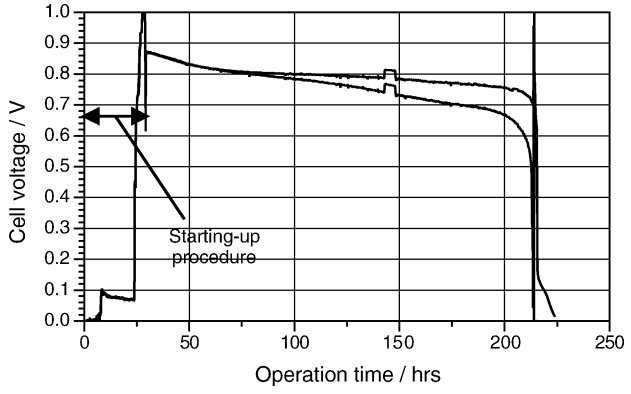

Fig. 2. Time dependence of the output voltage of a type A stack operated at 800 °C and with a constant load of 0.3 A cm^{-2}.

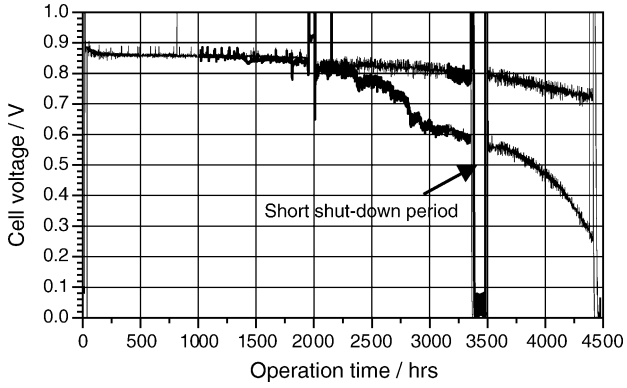

Fig. 3. Time dependence of the output voltage of a type B stack operated at 800 °C and with a constant load of 0.3 A cm^{-2}.

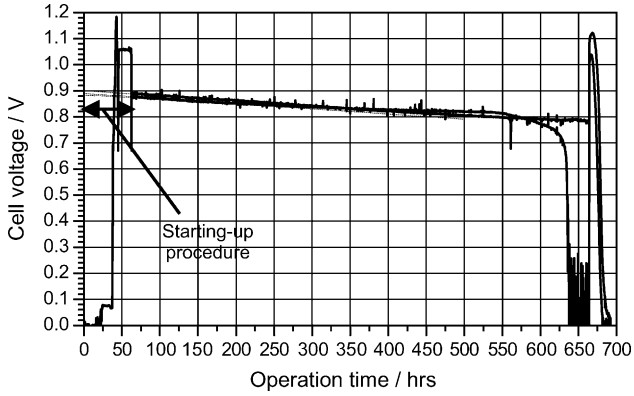

Fig. 4. Time dependence of the output voltage of a type D stack operated at 750 °C and with a constant load of 0.3 A cm^{-2}.

severe degradation only after a few thousand hours of operation at 800 °C (Fig. 3). The initial voltage under constant electrical load for these types of stacks was between 860 and 900 mV. During the first few tens of hours the stacks again showed a relatively high degradation rate decreasing the cell voltage to about 830–860 mV. After this initial period the stacks exhibited relatively stable operation with limited degradation rates. In Fig. 3, one cell of the type B stack shows a higher degradation rate after about 2000 h. After 3000 h progressive degradation of the other cell also starts. In the present case, the stack test was terminated after about 4200 h of operation with the OCV value still higher than 1000 mV at 800 °C. No short-circuiting was detected. Also type B and C stacks, which exhibited severe degradation after a few thousand hours of operation, ended with an ohmic resistance of about 5 Ω. Here, the OCV was much lower than the theoretical value.

Interestingly, the type D stack with a thin, protective ZrO_2 layer showed a sudden decrease of the cell output voltage, too. The lifetime ended after about 600 h of operation (Fig. 4). Although a progressive degradation of the electrochemical behaviour similar to type A stacks is observed, the OCV of both cells was higher than 1000 mV and no short-circuiting was measured between the interconnect and the coated frames.

3.2. Post-operation analysis: surface morphology

Optical examinations of type A stacks, for which short-circuiting after a few thousand hours of operation was characteristic, revealed that voluminous iron oxide nodules had been formed between two successive steel sheets. Fig. 5a shows the still intact type A stack after 2900 hours of operation at 700 °C. At the side face of the stack (Fig. 5b) the morphology of the outer rim of the glass–ceramic sealant becomes visible. A bright phase, rich in Ba, Cr and O formed as a side effect of the intended bonding reaction between the glass–ceramic and the steel. Similar observations were found by Yang et al. [3]. Of specific interest for the degradation effect is the presence of iron-rich oxide nodules formed between the two metallic sheets.

After removing the sealed cover plate from the stack and turning the plate upside down, iron-rich oxide nodules are observed in top view along the outer rim of the seal. Fig. 6a shows the inner surface (anode side) of the cover plate with the framed location of large iron-containing oxide nodules. Fig. 6b shows the reaction site at higher magnification. In some of the nodules also pure iron was detected. Further away from the seal rim the surface of the steel (air side) is covered by a homogeneous oxide layer, rich in chromium and manganese (see also Refs. [10,13,25]). On the oxide surface next

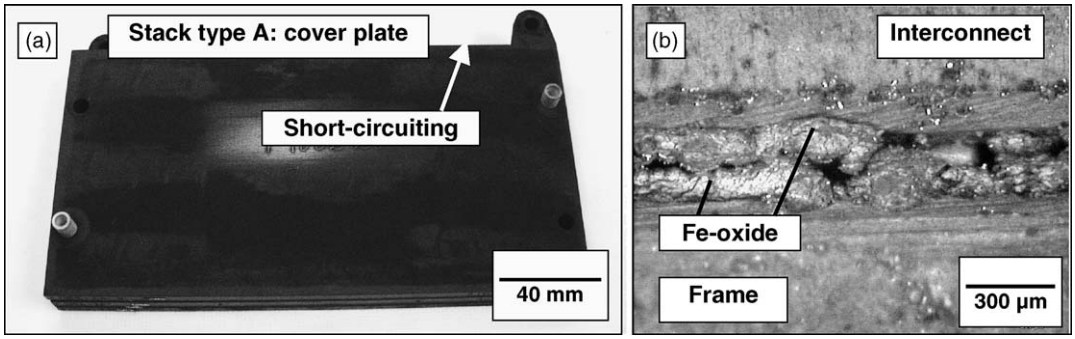

Fig. 5. SOFC stack of type A after 2900 h of operation at 700 °C: (a) top view of stack with cover plate and (b) side view into seal gap between metallic interconnect and frame. Formation of barium chromate and iron-containing oxide nodules at outer rim of seal (air side).

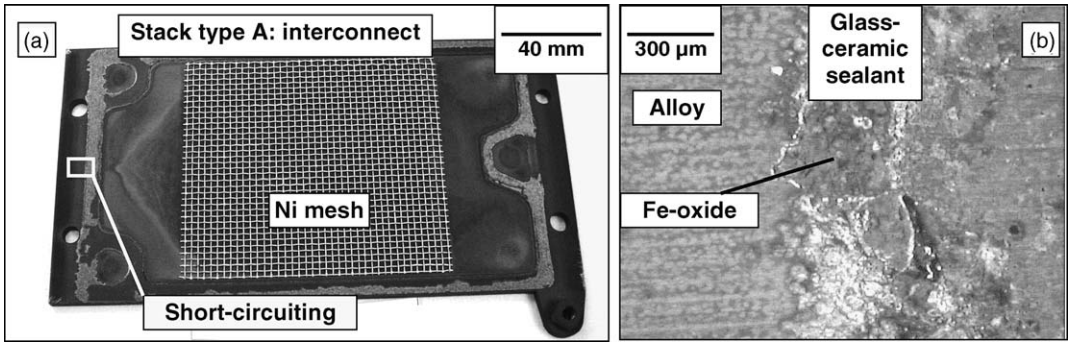

Fig. 6. Dismantled SOFC stack from Fig. 5 (a) anode side of interconnect and (b) magnified outer rim of glass–ceramic sealant. Formation of iron-containing oxide nodules.

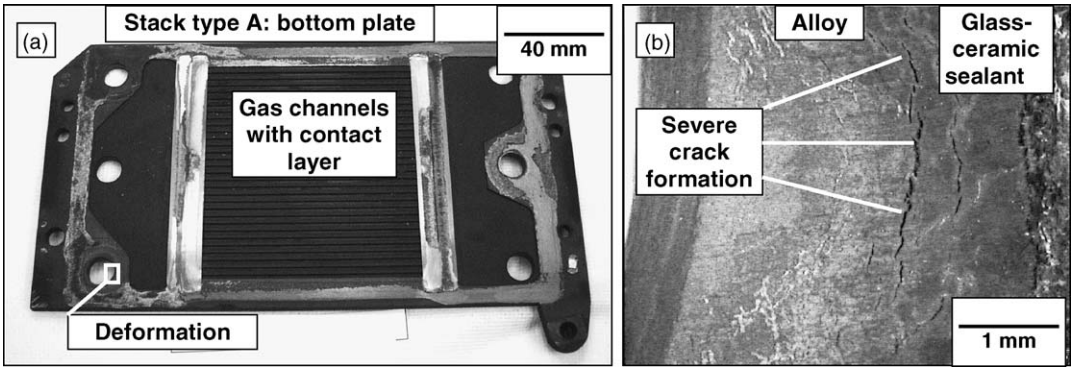

Fig. 7. Dismantled SOFC stack from Fig. 5 (a) bottom plate (cathode side) and (b) crack formation and bulging at inner rim of seal for fuel gas channel.

to the glass sealant spots also exist where small concentrations of Pb were detected. Besides the three-phase boundary of steel/glass–ceramic sealant/air another corrosion effect can be observed at the opposite rim of the glass–ceramic seal at the anode side (hydrogen side) and in the fuel gas channels. The steel surface adjacent to the seal rim appears bulged and contains cracks up to a distance of 2–4 mm. Fig. 7a shows a macrograph indicating a location with corrosion in the fuel gas channels. Fig. 7b depicts at higher magnification the severe crack formation on the steel surface near the glass–ceramic rim.

Fig. 8a illustrates a different corrosion situation related to the sealing of the fuel gas channels. The cathode side of a type A stack operated at 800 °C is displayed. Near the seal rim, separating the fuel gas from the oxidant, appreciable amounts of iron-containing nodules were found. At higher magnification (Fig. 8b) a seam of nodules is observed. In general the iron-containing nodules are similar in the stacks operated at 700 and 800 °C, but the exposure time needed for the formation of these nodules is a few thousand or a few hundred hours of operation, respectively.

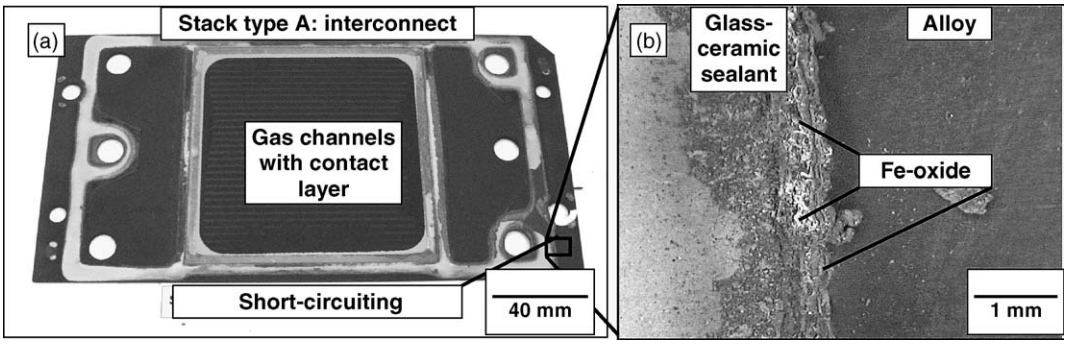

Fig. 8. Dismantled SOFC stack of type A after 300 h of operation at 800 °C: (a) interconnect (cathode side) and (b) formation of iron-containing oxide nodules at outer rim (air side) of gas channel seal.

Similar corrosion effects were also observed for the other stacks of type B, C, and D. However, the B and C type stacks operated at 800 °C only showed the same chemical interaction after a few thousand hours of operation.

Summarizing the post-operation surface examinations of the SOFC stacks, the following findings have to be emphasized:

(i) Highly conductive iron-containing oxide nodules were observed between the otherwise sealant-separated metallic sheets near the three-phase boundary of air/glass–ceramic sealant/steel.
(ii) Corrosion of the steel near the three-phase boundary of fuel gas/glass–ceramic sealant/steel was accompanied by bulging and crack formation.
(iii) The onset of severe performance degradation was correlated to the presence of iron-oxide-containing nodules. Distinct differences in the formation kinetics were observed as a result of changes in operation temperature and the chosen ferritic steel/glass–ceramic combination.

3.3. Post-operation analysis: cross section examination

The chemical interaction phenomena at both rims of the glass–ceramic sealant (air and fuel side) were further elucidated by cross-sectional examinations. Fig. 9 shows part of an interconnect component (type A stack) with a fractured glass–ceramic sealant on top. The sealant separates the fuel gas from air. The SEM micrograph focuses on the seal rim at the air side, where severe oxidation took place after a few thousand hours of operation at 700 °C. The internal and external oxidation with large outward-growing iron-rich oxide nodules is obvious. The internal oxidation is governed by chromia formation along the grain boundaries (intergranular) as well as at the inner part of the grains (intragranular). Note that the corrosion causes chromium depletion in the steel.

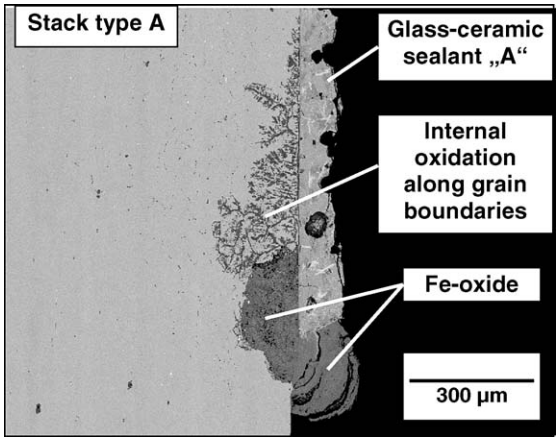

Fig. 9. SOFC stack of type A after 3450 h of operation at 700 °C. SEM micrograph of cross section showing interconnect with part of fractured glass–ceramic sealant still attached. Iron-containing oxide nodule at outer rim (air side).

Severe internal oxidation is also found at the three-phase boundary of hydrogen/glass–ceramic sealant/steel (Fig. 10). No large iron-rich oxide nodules are present but pronounced bulging is obvious. Although Figs. 9 and 10 show cross sections of stacks operated for a few thousand hours the results can be taken as representative of stacks with short-term degradation, too.

Once the nodules have grown to such an extent that they bridge the seal gap, a physical contact of the otherwise isolated steel components is established. To avoid this short-circuiting by conductive iron-containing oxide nodules, the surface of the cell frames in type D stacks was coated with a thin protective YSZ layer. The steel coated with the plasma-sprayed YSZ exhibited neither internal oxidation nor are external oxide nodules formed during the 600 h of stack operation at 750 °C (Fig. 11). However, the unprotected opposite surface of the interconnect showed severe corrosion. Since Fig. 11a covers the complete width of the seal, the advantage of the coating on the air and fuel side becomes obvious. At the uncoated air side, appreciable outward-growing iron-rich oxide nodules are found (Fig. 11b). The complete internal oxidation underneath the glass–ceramic sealant indicates that the fuel gas had access at operation temperature. The interfacial delamination crack between the glass–ceramic and the steel might have served as a path for fuel transport. The protective function of the YSZ coating and the pronounced internal oxidation of the steel are further confirmed in Fig. 12, which magnifies the area around the seal rim at the fuel side. The internal oxidation is accompanied by bulging of the steel and formation of surface cracks.

The cross-sectional observations demonstrated severe chemical interaction at the glass–ceramic steel interface resulting in internal and external oxidation. Also

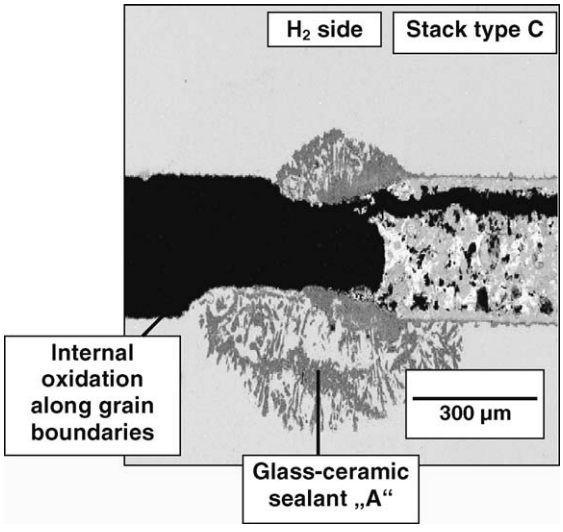

Fig. 10. SOFC stack of type C after 4200 h of operation at 800 °C. SEM micrograph of cross section showing seal of interconnect and cell frame at fuel side rim. Internal oxidation along grain boundaries causes pronounced bulging.

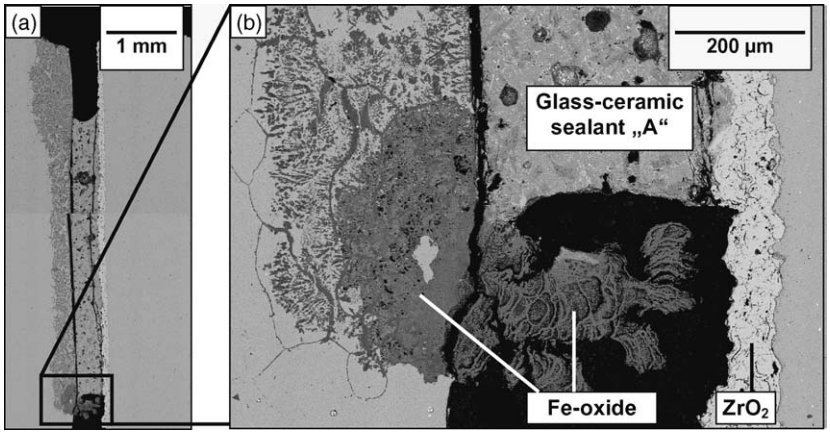

Fig. 11. SOFC stack of type D after 600 h of operation at 800 °C. SEM micrograph of cross section showing seal of gas channel between YSZ-coated cell frame and interconnect: (a) complete width of seal from fuel to outer ambient atmosphere. Internal oxidation underneath uncoated steel surface and presence of delamination crack along interface between glass ceramic and steel. (b) Fe-oxide formation.

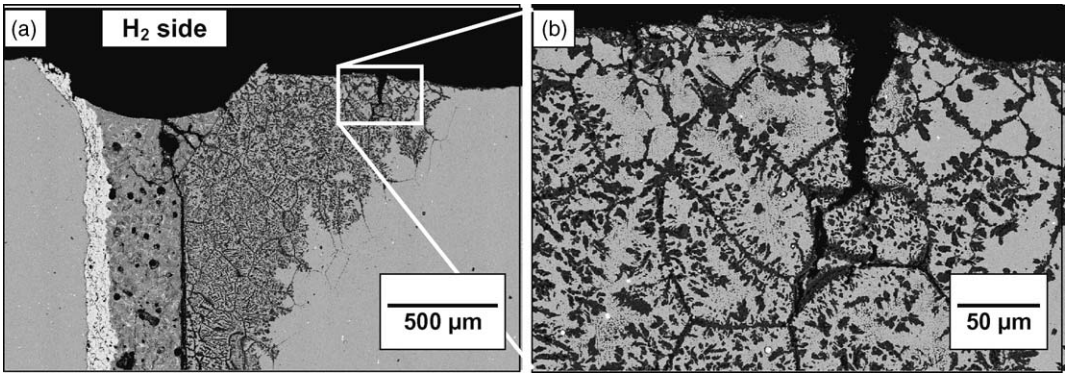

Fig. 12. Same SOFC stack as in Fig. 11. Asymmetric chemical interaction at inner rim of seal (fuel gas side). Internal oxidation along grain boundaries of steel and cracking. Internal oxidation completely suppressed by YSZ coating.

crack formation along the glass–ceramic/steel interface is observed. As expected, the operation temperature influenced the kinetics of the oxidation processes. In the case of type A stacks, only a few hundred hours of operation at 800 °C are sufficient for the excessive growth of oxide nodules. A reduction of the operation temperature to 700 °C led to a delay of the nodule growth rate by a factor of 10–20. With type B and C stacks, similar degradation shifts with respect to the steel composition are observed. The steel with the lower Si content (JS3) showed an incubation time to progressive degradation one order of magnitude longer (few thousand hours) than that for Crofer22APU-1st.

4. Discussion

The present study in combination with the results of other recent investigations [20–22] demonstrates that the onset of rapid degradation of SOFC stacks strongly depends on the chosen glass–ceramic/ferritic steel combination as well as on the operation temperature. Failure of the stacks was observed after short operation (few hundred hours) and long operation periods (few thousand hours). The electrochemical performance of the investigated stacks revealed:

- Type A stacks tested at 800 °C with an electrical load of 0.3 A cm^{-2} already showed severe performance degradation after 100–200 h. A reduction of the operation temperature to 700 °C postponed the onset of stack failure by a few thousand hours.
- Severe degradation of type B and C stacks tested at 800 °C with an electrical load of 0.3 A cm^{-2} started after several thousand hours of operation.
- A stack with YSZ-coated cell frames (type D) exhibited progressive degradation after 700 h of operation.
- The OCV values measured at the end of the stack lifetime were sometimes much lower than the theoretical value given by the Nernst equation. In these cases, the ohmic resistance at room temperature between the metallic frame and the interconnect steel turned out to be less than 5 Ω, indicative of short-circuiting. However, despite progressive degradation, in other cases, the OCV corresponded well to the theoretical value.

Post-mortem analyses (surface and cross-sectional) of those stacks that were shut down after severe degradation or failure showed interaction phenomena that could be distinguished with respect to reducing or oxidizing atmospheres at the opposite rims of the glass–ceramic seal.

- Strong internal oxidation of the steel occurred near the three-phase boundary between fuel gas, glass–ceramic sealant, and ferritic steel. The rapid internal chromia formation followed the grain boundaries (intergranular) and continued with dendritic growth towards the centre of the grains (intragranular). Such internal oxidation of the ferritic steel was also found at a lateral distance of 2–4 mm from the three-phase boundary. Moreover, severe internal oxidation of the ferritic steel was frequently found beneath the glass–ceramic sealant. Here, cracks were also present along the glass–ceramic/ferritic steel interface.
- Excessive internal oxidation of the ferritic steel under fuel conditions was accompanied by a substantial volume increase of the ferritic steel. Bulging of the steel was manifested as surface uplifts of up to several hundred microns. Locally, cracks were found on the steel surface.
- Internal and surface oxidation of the ferritic steel was found near the three-phase boundary between oxidant (air), glass–ceramic sealant and ferritic steel. Compared to the fuel gas side the internal oxidation (chromia formation) was generally less pronounced, but here voluminous outward growth of nodules rich in iron and oxygen dominated.
- The unwanted chemical interactions between the glass–ceramic and the ferritic steel could be successfully suppressed by applying a thin plasma-sprayed zirconia layer.

The stack test results described above can be compared with those of recent model experiments tailored to verify the interaction effect on a laboratory scale [20–22]. As was found in reproducible experiments, the rapid and massive internal oxidation as well as the iron oxide formation on the steel surface at the air side only occurred if glass–ceramic sealants contained minor amounts of PbO. The results also revealed that the Si content in the steel influenced the rate of attack. In the case of PbO-containing glass–ceramic sealants (“A”, “D”), it was found that increasing the Si content of the ferritic steel apparently increased the rate of corrosion attack. The operation time for type B and C stacks (ferritic steel with a Si content lower than 0.01 wt.%, and PbO-containing glass–ceramics “A” and “D”, respectively) is one order of magnitude higher than that of stacks of type A (ferritic steel with a Si content of 0.1 wt.%).

The onset of excessive interaction between the glass–ceramic sealant and the ferritic steel, as observed with stacks of type A, can also be slowed down by reducing the stack operation temperature. At 700 °C a comparable degradation of the electrochemical performance triggered by corrosion attack was observed only after several thousands of hours. Lowering the operation temperature apparently slowed down the reaction kinetics and increased the time of stable SOFC stack performance.

Based on the observed chemical interaction phenomena along with those from model experiments [20–22], the following sequential steps are suggested to govern the observed severe stack degradation and stack failure.

- The presence of hydrogen saturated with 3 vol.% water vapour favours the reduction of PbO into Pb. In this atmosphere, metallic Pb is the thermodynamically more stable phase and exists both as a liquid and vapour phase.
- Considering the low melting point and high vapour pressure, it is likely that Pb species are also found in the vicinity of the glass–ceramic seal. This assumption is backed by the internal oxidation distance from the glass–ceramic rim (2–4 mm).
- Pb reaching the steel surface contributes to the rapid severe internal oxidation of chromium, which resembles “liquid metal corrosion” [26–28]. The chromia formation proceeds fast along the grain boundaries and chromia-rich dendrites grow inside the grains.
- Internal oxidation with the formation of chromia results in a local volume increase of the ferritic steel. The bulging of the steel triggers delamination cracking along the interface between the glass–ceramic and the steel. As a wake effect, the fuel gas can penetrate into the crack and internal oxidation and swelling of the steel proceeds along the crack surface. The crack tip experiences higher stress intensity and thus moves further towards the opposite rim of the seal at the air side. Finally, delamination is completed and internal oxidation at the three-phase boundary between air, glass–ceramic, and ferritic steel is now also supported by the fuel gas. This bulging of the steel finally causes contact loss between the cathode and interconnect and/or between the anode and the Ni mesh, which adversely affects the overall electrochemical performance of the individual cells. At this stage, the OCV is not yet influenced. This also backed the findings that at the termination stage of certain stacks the performance was already significantly reduced whereas the OCV still corresponded to the theoretical value.
- Because chromium is continuously removed from the steel by the formation of chromia along the grain boundaries and chromia-rich dendrites inside the grains, the concentration of chromium in the bulk material is expected to decrease continuously. Once the critical concentration of ∼16% is reached [25], the steel is no longer able to form a chromia layer. Furthermore, the oxygen partial pressure at the air side is significantly higher than at the fuel side, and consequently, the growth rate of the iron-rich oxide nodules is high [29]. Eventually, the rapid formation of large Fe-oxide nodules with extremely small electrical resistance, especially Fe_3O_4 and FeO, will lead to “bridge” formation between two adjacent metallic sheets, and, as a result, to short-circuiting. The presence of the fuel gas

might in addition lead to a reduction of the iron oxide. At this short-circuiting stage, not only does a severe reduction of the electrochemical performance of the individual cells occur, but also the OCV is significantly lower than expected.

The present study and the follow-up investigations [20–22] have demonstrated that under SOFC conditions certain glass–ceramic/ferritic steel combinations may cause severe interaction, reflected by (i) excessive internal oxidation of the ferritic steel, (ii) crack formation along the glass–ceramic/steel interface, and (iii) fast outward-growing Fe-oxide nodules. These effects can be suppressed physically by a YSZ coating, which separates the glass–ceramic and the steel. Furthermore, glass–ceramics without PbO and ferritic steels with low Si content diminish the severe internal and external oxidation of the steel. However, from the experimental data no final conclusions can be drawn about the exact role of Pb and Si in the corrosion process. Further studies are necessary to understand the interaction mechanism and to elucidate the role of Pb and Si.

5. Conclusions

- Based on the observations of this study, a compositional incompatibility of glass–ceramic/ferritic steel combinations was identified as the origin of performance degradation of SOFC stacks.
- Severe chemical interaction causing accelerated corrosion of the ferritic steel only occurred under specific stack conditions including hydrogen and oxidant. Ultimately, the formation of highly conductive oxide nodules yielded material bridges which short-circuited the metallic cell frame and interconnect which were otherwise separated and isolated by the sealant.
- The results, together with those from recent investigations [20–22], indicate that minor elements in the glass ceramic and the steel caused the rapid internal corrosion of the steel. Besides protective steel coatings, e.g. plasma-sprayed YSZ, glass–ceramic sealants without PbO and ferritic steels with a low Si content provide promising material solutions for long-term operation of SOFC stacks.

Acknowledgements

The authors, members of the interdisciplinary “dissection group” at FZJ, would like to thank R. Steinberger-Wilckens as Head of the Fuel Cell Project for his continuous support of the post-operation stack analyses. Also the valuable contributions by several processing and characterization colleagues at FZJ, in particular R. Vassen, F. Tietz, L. Blum, H.W. Müskes, R. Erben, G. Blaß, M. Bram, S.M. Gross, and A. Cramer, are gratefully acknowledged.

References

[1] L.G.J. de Haart, I.C. Vinke, A. Janke, H. Ringel, F. Tietz, New developments in stack technology for anode substrate based SOFC, in: H. Yokokawa, S.C. Singhal (Eds.), Proceedings of the Solid Oxide Fuel Cells VII, vol. 16, Electrochemical Society, Pennington, USA, 2001, pp. 111–119.
[2] W.A. Meulenberg, N.H. Menzler, H.P. Buchkremer, D. Stöver, Manufacturing routes and state-of-the-art of the planar Jülich anode supported concept for solid oxide fuel cells, in: A. Manthiram, P.N. Kumta, S.K. Sundaram, G. Ceder (Eds.), Ceramic Transactions: Materials for Electrochemical Energy Conversion and Storage, 127, American Ceramic Society, Westerville, OH, 2002, pp. 99–108.
[3] Z. Yang, J.W. Stevenson, K.D. Meinhardt, Chemical interactions of barium–calcium–aluminosilicate-based sealing glasses with oxidation resistant alloys, Solid State Ionics 160 (2003) 213–225.
[4] K. Eichler, G. Solow, P. Otschik, W. Schaffrath, BAS (BaO–Al_2O_3–SiO_2)-glasses for high temperature applications, J. Eur. Ceramic Soc. 19 (1999) 1101–1104.
[5] S.B. Sohn, S.Y. Choi, G.H. Kim, H.S. Song, G.D. Kim, Stable sealing glass for planar solid oxide fuel cell, J. Non-Cryst. Solids 297 (2002) 103–112.
[6] T. Schwickert, P. Geasee, A. Janke, U. Diekmann, R. Conradt, Electrically insulating high-temperature joints for ferritic chromium steel, in: Proceedings of the International Brazing and Soldering Conference, Albuquerque, New Mexico, 2000, pp. 116–122.
[7] K.L. Ley, M. Krumpelt, R. Kumar, J.H. Meiser, I. Bloom, Glass–ceramic sealants for solid oxide fuel cells: Part I. Physical properties, J. Mater. Res. 11 (6) (1996) 1489–1493.
[8] Z. Yang, K.S. Weil, D.M. Paxton, J.W. Stevenson, J. Electrochem. Soc. 150 (9) (2003) A1188–A1201.
[9] K. Huang, P.Y. Hou, J.B. Goodenough, Characterisation of iron-based alloy interconnects for reduced temperature solid oxide fuel cells, Solid State Ionics 129 (2000) 237–250.
[10] Z. Yang, M. Walker, G. Xia, P. Singh, J.W. Stevenson, Anomalous corrosion behavior of stainless steels under SOFC interconnect exposure conditions, Electrochem. Solid-State Lett. 6 (10) (2003) B35–B37.
[11] T. Horita, Y. Xiong, K. Yamaji, N. Sakai, H. Yokokawa, Stability of Fe–Cr alloy interconnects under CH_4–H_2O atmosphere for SOFCs, J. Power Sources 118 (2003) 35–43.
[12] L. Jian, J. Huezo, D.G. Ivey, Carburisation of interconnect materials in solid oxide fuel cells, J. Power Sources 123 (2003) 151–162.
[13] P. Huczkowski, N. Christiansen, V. Shemet, L. Singheiser, W.J. Quadakkers, Growth rates and electrical conductivity of oxide scales on ferritic steels proposed as interconnect materials for SOFC, in: Proceedings of the Sixth European Solid Oxide Fuel Cells Forum, Mogensen (Ed.), Lucerne, Switzerland, 28 June–2 July, 2004, European Fuel Cell Forum, Oberrohrdorf, Switzerland, 2004, pp. 1594–1601.
[14] N. Sakai, T. Horita, Y. Xiong, K. Yamaji, H. Kishimoto, M.E. Brito, H. Yokokawa, T. Maruyama, Manganese chromium–iron-oxide in oxide scale of alloy interconnects, in: Proceedings of the Sixth European Solid Oxide Fuel Cells Forum, Mogensen, (Ed.), Lucerne, Switzerland, 28 June–2 July, 2004, European Fuel Cell Forum, Oberrohrdorf, Switzerland, 2004, pp. 1646–1653.
[15] R. Hojda, R. Heimann, W.J. Quadakkers, Production-capable materials concepts for high-temperature fuel cells, ThyssenKrupp Techforum, 2003, pp. 20–23.
[16] J. Piron-Abellan, F. Tietz, V. Shemet, A. Gil, T. Ladwein, L. Singheiser, W.J. Quadakkers, in: J. Huijsmans (Ed.), Proceedings of the Fifth European Solid Oxide Fuel Cell Forum, Lucerne, Switzerland, 2002, pp. 248–256.
[17] F. Tietz, D. Simwonis, P. Batfalsky, U. Diekmann, D. Stöver, Degradation Phenomena During Operation of Solid Oxide Fuel Cells, in: K. Nisancioglu (Ed.), Proceedings of the 12th IEA Workshop on

Materials and Mechanisms, Wadahl, Norway, Annex VII January, 1999, pp. 3–11.
[18] P. Batfalsky, H.-P. Buchkremer, D. Froning, F. Meschke, H. Nabielek, R.W. Steinbrech, F. Tietz, Operation and analysis of planar stacks, in: Proceedings of the Third IFCC, Nagoya, Japan, 1999.
[19] P. Batfalsky, R.W. Steinbrech, I.C. Vinke, E. Wessel, Analyses of SOFC stacks after electrochemical operation, in: J. Huijsmans (Ed.), Proceedings of the Fifth European Solid Oxide Fuel Cell Forum, Lucerne, Switzerland, 2002, pp. 837–846.
[20] V.A.C. Haanappel, V. Shemet, I.C. Vinke, S.M. Gross, Th. Koppitz, N. Menzler, M. Zahid, W.J. Quadakkers, Evaluation of the suitability of various glass sealant – steel combinations under SOFC stack conditions, J. Mater. Sci. 40 (2005) 1583–1592.
[21] V.A.C. Haanappel, V. Shemet, S.M. Gross, Th. Koppitz, N. Menzler, M. Zahid, W.J. Quadakkers, Behaviour of various glass–ceramic sealants with ferritic steels under simulated SOFC stack conditions, J. Power Sources 150 (2005) 86–100.
[22] N.H. Menzler, D. Sebold, M. Zahid, V. Shemet, S.M. Gross, Th. Koppitz, Interaction of metallic SOFC interconnect materials with glass–ceramic sealant in various atmospheres, J. Power Sources 152 (2005) 156–167.
[23] R. Steinberger-Wilckens, L.G.J. de Haart, I.C. Vinke, L. Blum, A. Cramer, J. Remmel, G. Blass, F. Tietz, W.J. Quadakkers, in: S.C. Singhal, M. Dokiya (Eds.), Proceedings of Solid Oxide Fuel Cells VIII, Paris, France, 27 April–2 May, The Electrochemical Society Inc, Pennington, USA, 2003, pp. 98–104.
[24] A. Mai, V.A.C. Haanappel, S. Uhlenbruck, F. Tietz, D. Stöver, Solid State Ionics 176 (2005) 1341–1350.
[25] W.J. Quadakkers, J. Piron-Abellan, V. Shemet, L. Singheiser, Mater. High Temperatures 20 (2) (2003) 115–127.
[26] V.Y. Abramov, S.N. Bozin, S.V. Evropin, B.S. Rodchenkov, V.N. Leonov, A.I. Filin, Proceedings of the 11th International Conference on Nuclear Engineering, Tokyo, Japan, 20–23 April, 2003, pp. 1–4, ICONE11 – 36413.
[27] G. Benamati, C. Fazio, H. Piankova, A. Rusanov, J. Nucl. Mater. 301 (2002) 23–27.
[28] V.E. Fradkov, Scripta Metall. Mater. 30 (12) (1994) 1599–1603.
[29] J. Zurek, M. Michalik, T.-U. Kern, L. Singheiser, W.J. Quadakkers, Oxidation of Metals 63 (5–6) (2005) 401–422.